Neutron powder diffraction and solid-state deuterium NMR studies of Ca_2RuD_6 and the stability of transition metal hexahydride salts

Ralph O. Moyer Jr. [a], Sytle M. Antao [b], Brian H. Toby [b],
Frederick G. Morin [c], Denis F.R. Gilson [c,*]

[a] *Department of Chemistry, Trinity College, Hartford, CT 06106-3100, United States*
[b] *Advanced Photon Source, Argonne National Laboratory, Argonne, IL 60439-4856, United States*
[c] *Department of Chemistry, McGill University, Montreal, Que. H3A 2K6, Canada*

Abstract

The crystal structure of Ca_2RuD_6 has been determined by neutron powder diffraction: space group $Fm3m$, K_2PtCl_6 structure, as found for other hexahydride salts of group 8 metals with alkaline earth or lanthanide counter ions. No structural phase transition was observed between 340 K and 50 K. The deuterium nuclear quadrupole coupling constant, 54.7 kHz, leads to an ionic character of the Ru–D bond of 76%. The known trends in the behaviour of A_2MH_6 salts are interpreted in terms of the ionization energies of the cation and the central metal atom.
© 2007 Elsevier B.V. All rights reserved.

Keywords: Ternary metal hydrides; Neutron diffraction; Deuterium NMR; Stability

1. Introduction

The ternary transition metal hydrides/deuterides (TMH/Ds) of the alkaline earth and lanthanide salts of iron, ruthenium and osmium hydrides, A_2MH_6, exhibit interesting structural and spectroscopic trends. The unit cell dimensions depend upon the ionic radii of the alkali metal and the metal–deuteride bond distances in the Fe, Ru, Os group and increase in the order Fe < Ru < Os, as expected. They also depend markedly on the counter-ion, with Mg < Ca < Sr < Ba for all salts in the series [1]. The complete structure of Ca_2RuD_6 has not been previously reported and is the subject of the present report, together with a deuterium solid-state NMR study of Ca_2RuD_6.

Kritikos and Noréus [2] have shown that the infrared active metal–hydrogen stretching modes depend on the unit cell dimension and attribute this to the size of the counter-ion, with electropositive character of the group 2 ion of only secondary importance. However, Parker et al. [3] in a study of alkali metal salts of $[PtH_6]^{2-}$ concluded that the alkali metal ion reduced the charge on the platinum and hydrogen, thus stabilizing the com-

plex. With this mechanism, the electropositive character of the counter-ion assumes much greater importance. Thus the inter-relationships between the bond lengths, unit cell dimensions and vibrational frequencies and the role of the electropositivity require attention and we suggest a more quantitative approach to these questions.

2. Experimental

Ca_2RuD_6 was prepared by the previously reported method [4] and the purity was confirmed by X-ray powder diffraction and infrared and Raman spectroscopy.

Neutron powder diffraction data were collected using the 32 detector BT-1 neutron powder diffractometer at the National Institute of Standards and Technology (NIST) Center for Neutron Research reactor, NBSR. The neutron diffraction data were modeled using the Rietveld method, as implemented in the *GSAS* and *EXPGUI* programs [5,6]. For the initial room temperature cubic structure, the starting atomic coordinates, cell parameters, isotropic displacement parameters, and space group, $Fm3m$, were taken from Moyer and Toby [7]. The Ca atom occurs on the 8c Wyckoff site, Ru at 4a, and D at 24e. The refined atomic coordinates were then used as input for the next structure at the different temperatures. The background was modeled using a 12-coefficient Chebyschev polynomial function. The reflection-peak profiles were fitted with three Gaussian coefficients (GU, GV, and GW). Individual isotropic displacement parameters were also refined. A full-matrix least-squares refinement with 4 structural parameters, one lattice constant and 17 experimental parameters (12 background terms, 3 profile parameters, a scale factor, and a zero shift) were allowed to vary simulta-

* Corresponding author.
E-mail address: denis.gilson@mcgill.ca (D.F.R. Gilson).

Table 1
Rietveld fit and structural parameters for Ca_2RuD_6

T (K)	a (Å)	D_z	U_{Ru} ($\times 100$ Å^2)	U_{Ca} ($\times 100$ Å^2)	U_D ($\times 100$ Å^2)	Ca–Ru (Å)	Ru–D (Å)	Ca–D (Å)	χ^2	R_F^2	R_{WP}	R_P
RT	7.2214(1)	0.2355(2)	0.40(5)	0.46(5)	2.11(3)	3.12697(4)	1.700(2)	2.5553(1)	1.399	0.0485	0.0720	0.0578
348	7.2300(1)	0.2359(2)	0.45(5)	0.77(5)	2.32(4)	3.13067(4)	1.706(2)	2.5582(1)	1.356	0.0464	0.0666	0.0529
RT	7.2226(1)	0.2359(2)	0.38(5)	0.64(5)	2.05(3)	3.12749(4)	1.704(2)	2.5556(1)	1.441	0.0498	0.0696	0.0546
50	7.1985(1)	0.2374(2)	0.03(6)	0.12(4)	1.37(3)	3.11702(3)	1.709(2)	2.5467(1)	2.199	0.0495	0.0670	0.0509

Ca is at (1/4,1/4,1/4), Ru is at (0,0,0) and D is at (0,0,z).

neously to convergence. A test refinement of the deuterium atom site occupancy gave a result consistent with Ca_2RuD_6 with full occupancy on all sites and very high isotopic purity, so this parameter was fixed at unity. The number of observed reflections in a typical dataset is 38, and the number of observations (data points) is about 2890. Diffraction data were collected initially at room temperature, then at 348 K, again at room temperature and finally at 50 K.

Deuterium NMR spectra were obtained at room temperature using a Chemagnetics CMX-300 spectrometer at an operating frequency of 45.9 MHz, using the quadrupole-echo method [8] for static spectra with a pulse width of 4 μs and refocusing time of 25 μs, and 56 scans were acquired with a recycle time of 600 s. Magic-angle-spinning (MAS) spectra were obtained using a 7 mm probe, 3 μs pulse width and 24 acquisitions with a pulse delay of 600 s at a spinning rate of 4.0 kHz.

3. Results and discussion

3.1. Rietveld structure refinements

Table 1 contains the refinement agreement and structural parameters for Ca_2RuD_6. As an example, the fit for the room temperature data set is shown graphically in Fig. 1. Diffraction results indicate that Ca_2RuD_6 remains cubic (K_2PtCl_6 structure) within the temperature range 348–50 K. These results are consistent with other six-coordinate transition metal hydrides of the formula A_2MH_6, where there are no structural phase transitions at low temperatures. The size of the unit cell, 7.222(3) Å, is intermediate between those of the magnesium and strontium salts and agrees well with the value of 7.24 Å
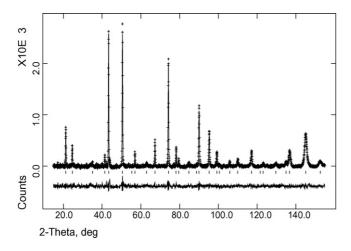
reported previously for the X-ray diffraction study [4] of Ca_2RuH_6.

3.2. Deuterium NMR

The static ^2H NMR spectrum for Ca_2RuD_6 showed a Pake doublet with a weak central peak, Fig. 2. The magic-angle-spinning (MAS) spectra showed that this peak had an intensity of about 5% of the total area and is attributed to impurities. On annealing the sample at 348 K, the intensity of the impurity peak decreased to 3%. The spacing between the "horns" of a Pake doublet equals $(3/4)C_Q$, where C_Q is the deuterium quadrupole coupling constant, e^2Qq/h, Q is the nuclear quadrupole moment and q the electric field gradient. A value of 54.7 kHz was obtained, indicating that the structure is rigid at room temperature in agreement with the neutron diffraction results. In contrast, high molecular mobility has been reported for the hexahydrido-platinate salt K_2PtH_6 [9].

Berke and co-workers [10–12] have interpreted the deuterium quadrupole coupling constants in metal hydrides in terms of the
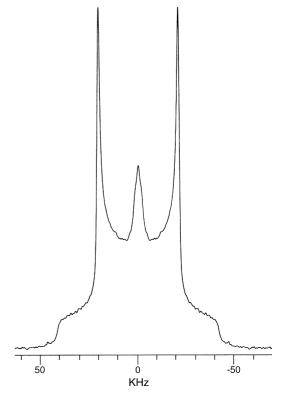

Fig. 1. Observed (continuous line) and calculated (crosses) neutron powder diffraction data for Ca_2RuD_6 at room temperature. The difference curve ($I_{obs} - I_{calc}$) is shown at the bottom. The short vertical lines indicate positions of allowed reflections.

Fig. 2. Room temperature deuterium NMR spectrum of Ca_2RuD_6.

Table 2
Ionization energy (eV), unit cell dimensions (Å) and vibrational wavenumber (cm^{-1})

	Mg	Ca	Sr	Ba	Eu	Yb	Fe	Ru	Os
IE(I)	7.646	6.113	5.696	5.212	5.670	6.254	7.902	7.361	8.438
IE(II)	15.035	11.872	11.030	10.004	11.25	12.179			
a_0 Ru	6.6294	7.2220[a]	7.6088	8.0283	7.557[b]	7.248[b]			
a_0 Os	6.6734	7.2361	7.626[b]	8.0246					
ν(Ru–H)	1783	1564	1487	1438	1462	1550			
ν(Ru–D)	1279	1128	1075	1023	1064				
ν(Os–H)	1849	1637	1575	1505					
ν(Os–D)	1325			1078					

Data from Refs. [2,4,17–20].

[a] Present work.

[b] Hydrides.

ionic character of the metal–hydrogen bonds. According to the Townes and Dailey treatment [13], the molecular field gradient q_{mol} is given by the following Eq. (1):

$$q_{mol} = (1 - s)(1 - I)q_{at} \qquad (1)$$

where s is the s-character, I is the ionic character of the deuterium–metal bond and q_{at} is the atomic field gradient. By substituting the appropriate quadrupole coupling constants for the field gradients, the ionic character of the bond is given by the following Eq. (2):

$$I = \frac{1 - (C_Q)_{M-D}}{(C_Q)_{D-D}} \qquad (2)$$

Using a nuclear quadrupole coupling constant for D_2 of 227 kHz (where the ionic character is zero), a value of 76% was obtained for the ionic character. This is in the same range as the values of 78 and 89% and 70 and 82% obtained in an earlier study [14] for the equatorial and apical deuterium positions in Ca_2IrD_5 and Ca_2RhD_5, respectively, for the rigid low temperature phases of these compounds. Clearly, these metal–hydrogen bonds retain a high degree of ionic character. For the $[PtH_6]^{2-}$ complexes, a largely covalent bond was predicted [3].

3.3. Origin of the dependence on the counter-ion

It is well known that for the group 8 metal hexahydride complexes, the unit cell dimensions, a_0, the M–D bond lengths and metal–hydrogen vibrational wavenumbers are all dependent on the nature of the alkaline earth or lanthanide counter-ion, Table 2, but no quantitative basis for these trends has been established. In their studies of the vibrational spectra of Rb_2PtH_6 and Rb_2PtD_6, Parker et al. used density functional theory (DFT) calculations to confirm the vibrational assignments and extended these calculations to the whole series of alkali metal salts [3]. They concluded (a) that the alkali metal counter-ion stabilizes the complex by removing charge from the transition metal and hydride ligand and (b) that the amount of charge depends upon the electropositivity of the alkali metal. A high electropositivity is equivalent to a low ionization energy and so we use the second ionization energy of the alkaline earth or lanthanide, i.e. the energy required to remove the second electron and give the A^{2+} cation [15], as a measure of the electropositivity. The wavenumbers assigned to

the metal–hydrogen antisymmetric T_{1u} stretching vibrations can be correlated with unit cell size [2,16]. Following the arguments of Parker et al., the spectroscopic properties should also correlate with the electropositive character of the counter-ion. As Fig. 3 shows, excellent linear relationships exist for the hydrogen and deuterium vibrational wavenumbers of both ruthenium and osmium complexes and the second ionization energy of their respective alkaline earth/lanthanide counter-ions. Others have suggested that the hydrogen distributes electron density away from the central metal atom and that the real electron population in the valence shell of a transition metal is very likely that of its atomic state [2]. If the wavenumbers are plotted versus the sum of the second ionization energy for the alkaline earth/lanthanide element and the first ionization energy of the transition metal, then the lines merge to give common lines for the M–H and M–D frequencies for both transition metals, Fig. 4. The R^2 factors were 0.992 and 0.993. The slopes of the lines, 0.0087 ± 0.00027 and 0.0064 ± 0.00023, and the intercepts, $211.7 \pm 43.0\,cm^{-1}$ and $143.5 \pm 36.3\,cm^{-1}$ for the hydride and deuteride curves, respectively, have ratios of 1.38 and 1.47, close to the value of $\sqrt{2}$ expected from the isotopic masses. The
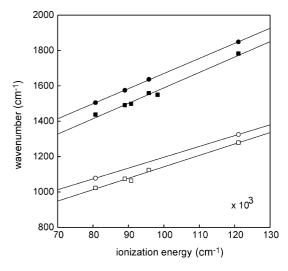

Fig. 3. Plot of vibrational wavenumber vs. the second ionization energy (converted to cm^{-1}) of the alkaline earth or lanthanide. Squares: Ru salts; circles Os salts, filled symbols for metal–hydrogen stretching frequencies and empty symbols for deuterium.
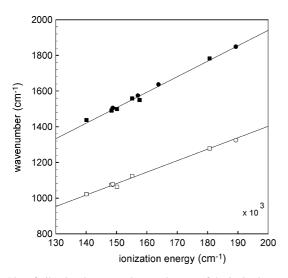
Fig. 4. Plot of vibrational wavenumber vs. the sum of the ionization energies (converted to cm^{-1}) of the alkaline earth or lanthanide and the transition metal. Squares: Ru salts; circles Os salts, filled symbols for metal–hydrogen stretching frequencies and empty symbols for deuterium.

occurrence of a common line differs from the plot of frequency versus unit cell dimension [2] where separate lines were found for each transition metal salt.

This close relationship between the vibrational wavenumber and the ionization energy confirms that the electropositivity of the alkaline earth and lanthanide counter-ions is a major factor in determining the solid-state structures of these TMH/D compounds. That the antisymmetric T_{1u} vibrations correlate with the ionization energies suggests that the induced dipole might mediate the transfer of charge. This could account for why the wavenumber and not the force constant is involved. Unfortunately, too few Raman-active totally symmetric A_{1g} stretching modes have been reported to test if a similar relationship occurs although the wavenumbers of these modes do depend upon the unit cell dimensions.

References

[1] R. Bau, M.H. Dabnis, Inorg. Chim. Acta 259 (1997) 27.
[2] M. Kritikos, D. Noréus, J. Solid State Chem. 93 (1991) 256.
[3] S.F. Parker, S.M. Bennington, A.J. Ramirez-Cuesta, G. Auffermann, W. Bronger, H. Ferman, K.J.P. Williams, T. Smith, J. Am. Chem. Soc. 125 (2003) 11656.
[4] R.O. Moyer Jr., C. Stanitski, J. Tanaka, M.I. Kay, R. Kleinberg, J. Solid State Chem. 3 (1971) 541.
[5] A.C. Larson, R.B. Von Dreele, General Structure Analysis System (GSAS), Los Alamos National Laboratory Report, LAUR, 2000, pp. 86–748.
[6] B.H. Toby, EXPGUI, a graphical user interface for GSAS J. Appl. Crystallogr. 34 (2001) 210–221.
[7] R.O. Moyer Jr., B.H. Toby, J. Alloys Compd. 363 (2004) 99.
[8] J.H. Davis, K.R. Jeffrey, M. Bloom, M.I. Valic, T.P. Higgs, Chem. Phys. Lett. 42 (1976) 390.
[9] D. Bublitz, G. Peters, W. Preetz, G. Auffermann, W. Bronger, Z. Anorg. Allg. Chim. 623 (1997) 184.
[10] H. Jacobsen, H. Berke, in: M. Peruzzini, M. Poli (Eds.), Recent Advances in Hydride Chemistry, Elsevier, The Netherlands, 2001 (Chapter 4).
[11] V.I. Bakhmutov, in: M. Peruzzini, M. Poli (Eds.), Recent Advances in Hydride Chemistry, Elsevier, The Netherlands, 2001 (Chapter 13).
[12] D. Nietlispach, V.I. Bakhmutov, H. Berke, J. Am. Chem. Soc. 115 (1993) 9191.
[13] C.H. Townes, B.P. Dailey, J. Chem. Phys. 17 (1949) 782.
[14] D.F.R. Gilson, F.G. Morin, R.O. Moyer Jr., J. Phys. Chem. B 110 (2006) 16487.
[15] http://physics.nist.gov/PhysRefData/Handbook/.
[16] R.O. Moyer, J.R. Wilkins, P. Ryan, J. Alloys Compd. 290 (1999) 103.
[17] J.S. Thompson, R.O. Moyer Jr., R. Lindsay, Inorg. Chem. 14 (1975) 1866.
[18] R. Lindsay, R.O. Moyer Jr., J.S. Thompson, D. Kuhn, Inorg. Chem. 15 (1976) 3050.
[19] B. Huang, F. Bonhomme, P. Selvam, K. Yvon, P. Fischer, J. Less Common Met. 171 (1991) 301.
[20] M. Kritikos, D. Noréus, B. Bogdanovic, U. Wilczok, J. Less Common Met. 161 (1990) 337.